Article

Assessment of the Overall Efficiency in WPT Stations for Electric Vehicles

Mauro Zucca [1,†], Vincenzo Cirimele [2,†], Jorge Bruna [3,†], Davide Signorino [1,†], Erika Laporta [3,†], Jacopo Colussi [2,*,†], Miguel Angel Alonso Tejedor [3,†], Federico Fissore [1,†] and Umberto Pogliano [1,†]

[1] Istituto Nazionale di Ricerca Metrologica (INRiM), 10135 Torino, Italy; m.zucca@inrim.it (M.Z.); d.signorino@inrim.it (D.S.); f.fissore@inrim.it (F.F.); u.pogliano@inrim.it (U.P.)

[2] Dipartimento Energia, Politecnico di Torino, 10129 Torino, Italy; vincenzo.cirimele@polito.it

[3] CIRCE Foundation, 50018 Zaragoza, Spain; jbruna@fcirce.es (J.B.); elaporta@fcirce.es (E.L.); maalonso@fcirce.es (M.A.A.T.)

* Correspondence: jacopo.colussi@polito.it

† These authors contributed equally to this work.

Abstract: The on-site assessment of the efficiency of a charging station is not a trivial process and is a topic of discussion for professionals. The efficiency of electric Vehicle Supply Equipment (EVSE), is an important parameter for both the user and the EVSE operator. This paper deals with a particular type of EVSE, using static wireless power transfer (WPT). This paper proposes a clear method to account for the parameters which can affect the correct determination of efficiency, such as in particular the accuracy of the meters and the effect of temperature. This work proposes a method to define the accuracy of the power and efficiency on-site assessment, and is aimed at clarifying that despite distorted waveforms at the charging stations, it is possible to reach a good accuracy in a wide temperature span (expanded uncertainty <0.5% between 5 °C and 40 °C). Analysis initiated from the measurement conditions and the actual waveforms recorded at two WPT EVSEs with differently rated power. This paper paves the way for the possibility of verifying class 0.5 m on-site, desirable for this type of application. The paper also clarifies that despite the evident presence of voltage and current ripple at the batteries, the weight of the ripple power on the total power is nevertheless lower than 0.1%. Finally, the paper highlights how, for the correct measurement of the ripple, it would be advisable to calibrate the instrumentation in DC and in AC, at a frequency double that of the working frequency of the EVSE coils.

Keywords: electric vehicles; inductive charging; measurement uncertainty; power system measurements

1. Introduction

Electric vehicles are gaining relevance in the recent years stimulating research in many different technical aspects [1–3]. The possibility that electric vehicles could reduce CO_2 emissions, and thus can represent a lever for decarbonisation, is an interesting perspective. A panorama of the current situation is well outlined in [4], which emphasizes the fact that the carbon footprint of the charging stations will also depend on the adoption of alternative energy sources. From a strictly technical point of view, regardless of energy sources, the aspects related to the efficiency represent in any case a crucial issue for electric vehicles (EVs) both for charging and for driving [5]. For charging, a novel category of stations (CSs) for EVs is entering the market and promises interesting developments, both for the intrinsic convenience of charging and for the prospects of pairing with autonomous driving. In inductive charging [6,7] energy transfer occurs wirelessly, through two resonant coils at a frequency ranging from ten to one hundred kilohertz. The coils are linked to AC-DC converters both on-board and on the ground, where there is also an AC-DC converter. As this is a relatively new technology, there are various open issues on this matter such as the optimization of the transmission efficiency and an integrated approach

between the electric grid and the CSs [8]. This paper provides a novel contribution to the solution of the problem of accurately measuring the electrical quantities in operating conditions, particularly power and efficiency of WPT CSs, which is a topic directly linked to CSs performance and billing. Modern billing systems are constantly evolving and it is reasonable to think that in many countries, this technology is moving towards interoperable systems in which the user can recharge at any station by paying for the cost of the energy transferred [9]. According to the standard IEC 61851-1, in the following, we will also call the charging station as electric vehicle supply equipment (EVSE), which is more common in industrial environment. In recent years, research on plug-in EVSE has intensified and has resulted in numerous scientific works, among which [10–13]. With the opening of the charging market to "pay-as-you-go", the design and accurate measurement of the efficiency of EVSE will also gain importance [14]. Reasonably, efficiency will become a parameter for the choice of a specific station by the charging-plant manager. The measurement of the efficiency of an EVSE involves the accurate measurement of the DC plus AC ripple power at the batteries, and the simultaneous measurement of the power absorbed from the electrical grid. Indeed, despite the improvement of power electronic converter performance, the measurement of the power at the batteries is still affected by a significant ripple. The harmonic noise produced by the chargers is determined by the characteristics of on-board and grid converters together with their interaction with the electrical grid. Suitable filters are designed to limit such harmonic noise, but a non-negligible AC ripple remains in the DC voltage and current at the batteries [15]. Moreover, the actual measurement of the power transferred from the grid to the vehicle involves the AC measurement in the resonant circuit, with an adequate choice of the instrumentation bandwidth. A first measurement system of the power transferred from the transmitter (Tx) coil to the receiver (Rx) coil was proposed in [16]. An ad hoc measurement system has been proposed by the authors in [17,18] in order to have accurate and traceable measurements of the electrical quantities on-board and on the grid side at WPT EVSE, as well as of the transmission efficiency with an expanded measurement uncertainty, at room temperature, lower than or equal to 10^{-3}. High-powered EVSE, for example for trucks or buses, necessarily require an on-site verification with the desirable presence of the vehicle (an equivalent load for such a power is rarely available). Moreover, a large EVSE cannot be placed in a climatic room in a laboratory to assess the temperature effect on the electrical quantities, the harmonic distortion effect and efficiency assessment [19]. This paper moves from two of the four measurement systems described in [17,18], one for on-board measurements and one for grid measurements, aiming at establishing a method to define the accuracy of on-site measurements. This paper proposes a clear procedure to assess the accuracy of the efficiency measurements in WPT EVSE. The proposed method takes into account the effect of temperature on the measurements system when measuring real waveforms (i.e., in presence of harmonic distortion). The methodology is explained in detail and provides a literature reference necessary for the physicists and engineers, albeit not expert in measurement science, to correctly evaluate the efficiency of a WPT EVSE. In particular, this paper discusses the temperature range in which it is possible to obtain, during in-field measurements, an accuracy similar to that obtainable in the laboratory ($\leq 10^{-3}$). Accuracy at room controlled temperature was previously verified trough the calibration in a new facility at Physikalisch-Technische Bundesanstalt (PTB), the German national metrological institute (NMI) in the framework of the Micev project [20,21]. Likewise, this paper aims to provide a similar analysis with regard to the measurements in the resonant circuit. Finally, this work aims to establish whether the measurable voltage and current ripple at the batteries has a significant effect on the measured power, also providing suggestions on the calibration of power analyzers dedicated to this task.

The structure of this paper is shown in Figure 1, which highlights the logical and functional links between the content of the various sections.
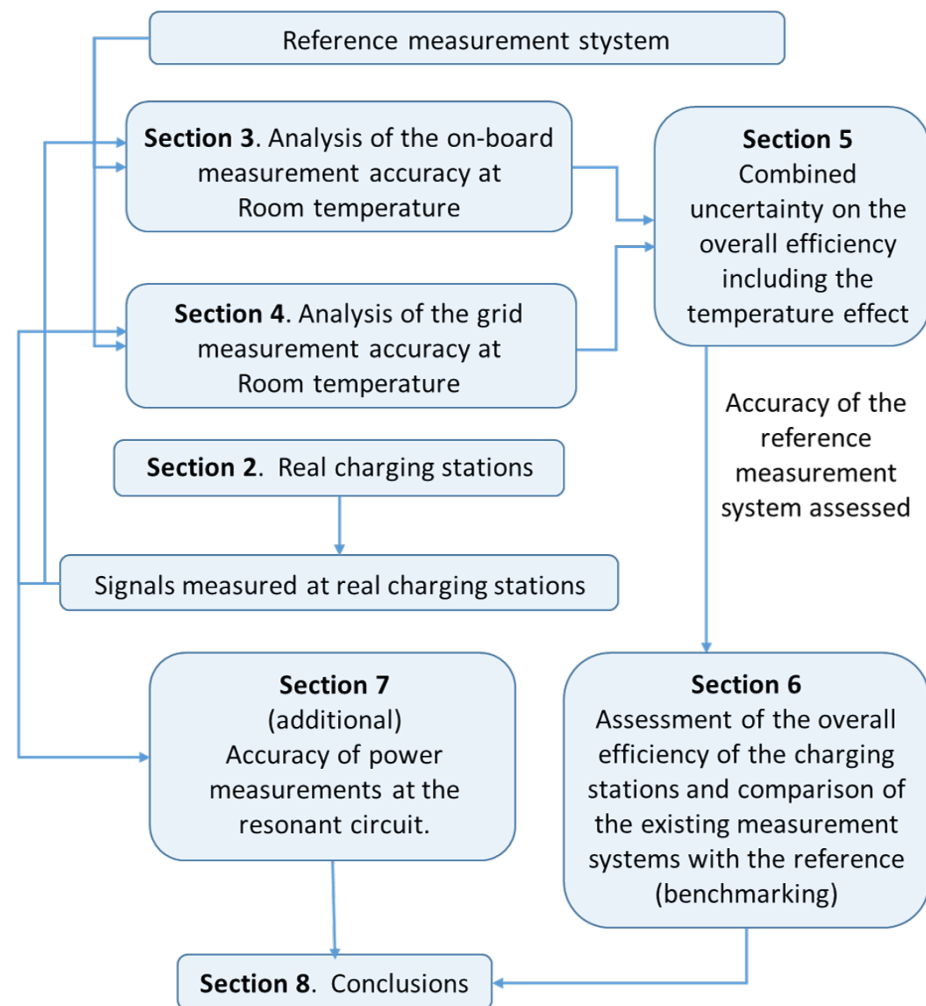
Figure 1. Logical and functional links between the contents of the various sections of the work.

2. Test EVSE and Efficiency

The evaluation of the measurement accuracy, in on-site efficiency and power measurements, needs to operate on real waveforms by evaluating their amplitude, frequency and harmonic distortion. For this purpose, two EVSE were arranged as test-benches for measurements.

2.1. Test EVSE

The first CS was made available by Circe Foundation, and in the following is called "Heavy vehicle" CS (HVCS). This system included a triple charging modality: conventional conductive charging, static inductive charging and dynamic inductive charging [15,22,23]. The static inductive power transfer (IPT) charging mode is the WPT of interest for this paper. The station rated power was 50 kW, but was limited to about 27.5 kW during measurements for thermal reasons, because of the continuous operations and repeated tests. The station included a Gulliver U520 ESP minibus 100% electric, hosting a receiving resonant coil sized 2.5 m × 0.4 m, below the chassis. The transmitter resonant coil size was 0.8 m × 0.4 m. The resonance frequency during measurements was 27.9 kHz. The battery rated voltage was 350 V but, to avoid damaging it due to the repeated on/off cycles of the system during the tests, an equivalent resistive load was used during measurement limiting voltages to about 225 V. A picture of the station is shown in Figure 2.

Figure 2. Facility made available by CIRCE Foundation for measurements. Heavy vehicle charging station. Detail of the minibus and of the resonant coils: transmitter coil and receiver coil.

The second charging station was made available by the Politecnico di Torino, and in the following is called "Light vehicle" CS (LVCS). This system was designed for dynamic inductive charging and tested on a full electric van along a dedicated charging lane, in the framework of the Fabric Project [24]. For this investigation, the system was mounted on a laboratory setup in order to perform static charging, as shown in Figure 3. Rated power of the system was 11 kW, but also in this case, due to continuous operations and repeated tests, it was limited to 3 kW during measurements. The resonance frequency of the whole system was 85 kHz.
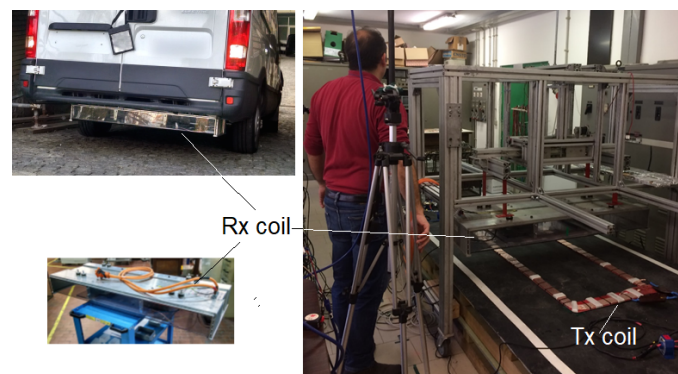
Figure 3. Facility made available by Politecnico di Torino for measurements. Light vehicle charging station laboratory setup. Detail of receiver coil mounted on the vehicle, dismounted and setup in the laboratory LVCS.

2.2. Measurement Points and Efficiency

Power transfer efficiency is the ratio between two electrical power quantities measured at the same time instant: the power measured on-board at the batteries, P_{board} in the following, and the power adsorbed and measured at the electrical grid, which is commonly a three-phase power called P_{grid} in the following. The overall efficiency is defined as $\mu = P_{board} / P_{grid}$. As regards the measurement on board, referring to the scheme in Figure 4, the measurement is made, if accessible, at point E, or at point D. As regards the measurement of the connection with the electrical network, this is done at point A. Starting from the above definitions, if the measurements of the two powers can be considered uncorrelated, as reasonably it is, the uncertainty on the measurement of the efficiency can be obtained through the Formula (1) [25]:

$$u_{\mu}^2 = \mu^2 \cdot \left[\left(u_{rP_{grid}} \right)^2 + \left(u_{rP_{board}} \right)^2 \right] \tag{1}$$

where u_μ is the measurement uncertainty on the overall efficiency, $u_{rP_{grid}}$ is the measurement relative uncertainty on the measured power from the grid and $u_{rP_{board}}$ is the measurement relative uncertainty on the measured power at the batteries. In this analysis, the target measurement uncertainty on overall efficiency is 10^{-3}.

Figure 4. Simplified scheme of a IPT charging station.

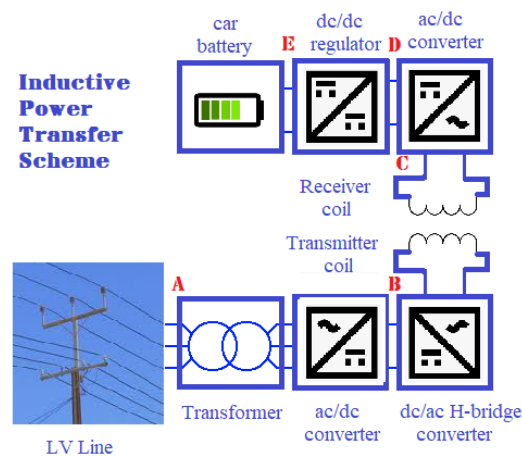To define the measurement overall efficiency uncertainty, four measurements were chosen; two carried out at LCVS and two carried out at HVCS, in two different load conditions, hereinafter referred to as load condition #1 and load condition #2. Each measurement consists of two synchronized results: one obtained on-board (point E) and one obtained at the grid (point A). Table 1 reports the results, for each station and each measurement condition, in two lines: the first line shows the main quantities magnitude (i.e., r.m.s value) at the batteries, where AC quantities refer to the ripple; the second line shows the r.m.s value of currents, voltages and power adsorbed from the grid. Further measurements are reported in Section 6.

Table 1. Synchronized measurements on-board and at the grid. r.m.s. values of currents in (A), voltages in (V) and power in (W). Letters ρ, σ and τ identify the grid phases.

	n	I_{DC}	U_{DC}	I_{AC}	V_{AC}	P_{DC}	$\cos\phi_b$	I_ρ	I_σ	I_τ	U_ρ	U_σ	U_τ	P_{tot}	$\cos\phi_g$
LVCS	#1	27.40	97.53	1.28	0.81	2672.50	0.9989	5.138	4.910	4.931	381.52	383.40	384.85	3003.5	0.9064
LVCS	#2	8.65	349.76	0.70	0.81	3027.14	0.9967	5.143	4.915	4.953	382.22	384.81	385.47	3015.9	0.9060
HVCS	#1	65.8	156.8	0.80	1.78	10,321.1	0.9999	20.44	20.05	19.81	234.04	235.44	233.21	14,111.9	0.9990
HVCS	#2	76.2	182.4	6.94	1.96	13,891.8	0.9959	26.66	25.50	25.35	232.79	233.87	232.76	17,814.45	0.9987

3. DC Measurements On-Board and Parameters of Uncertainty

3.1. DC Measurements

Measurements at the DC load (batteries) were performed on both stations. The maximum values of voltage, current, and transferred power recorded during the measurements, at the DC load (point E), are shown in Table 2. The recorded values show a voltage and current ripple which, reasonably, is attributable to the converters and disturbances deriving from power electronics [26]. In [21] the authors already reported the measured waveforms referred to the LVCS. Here, in Figure 5, we report the waveforms referred to the HVCS. In both cases it is possible to notice that the voltage and current ripple has a frequency double than the one of the resonant circuit (55.8 kHz compared to 27.9 kHz in the case of Figure 5), due to the effect of the passive diode rectifiers. Considering the worst case of the first harmonics of current and voltage in phase, in the case of Figure 5 the power associated with the ripple is equal to 0.472 W being the 0.002% of the power measured on board, this latter being equal to 20.93 kW. The power associated with the ripple is therefore negligible and even though it tends to increase by reducing the nominal power of the station and the

power transferred, in the author measurement experience it is always much lower than 0.1% of the transferred power.

Table 2. Maximum on-board quantities measured at the stations.

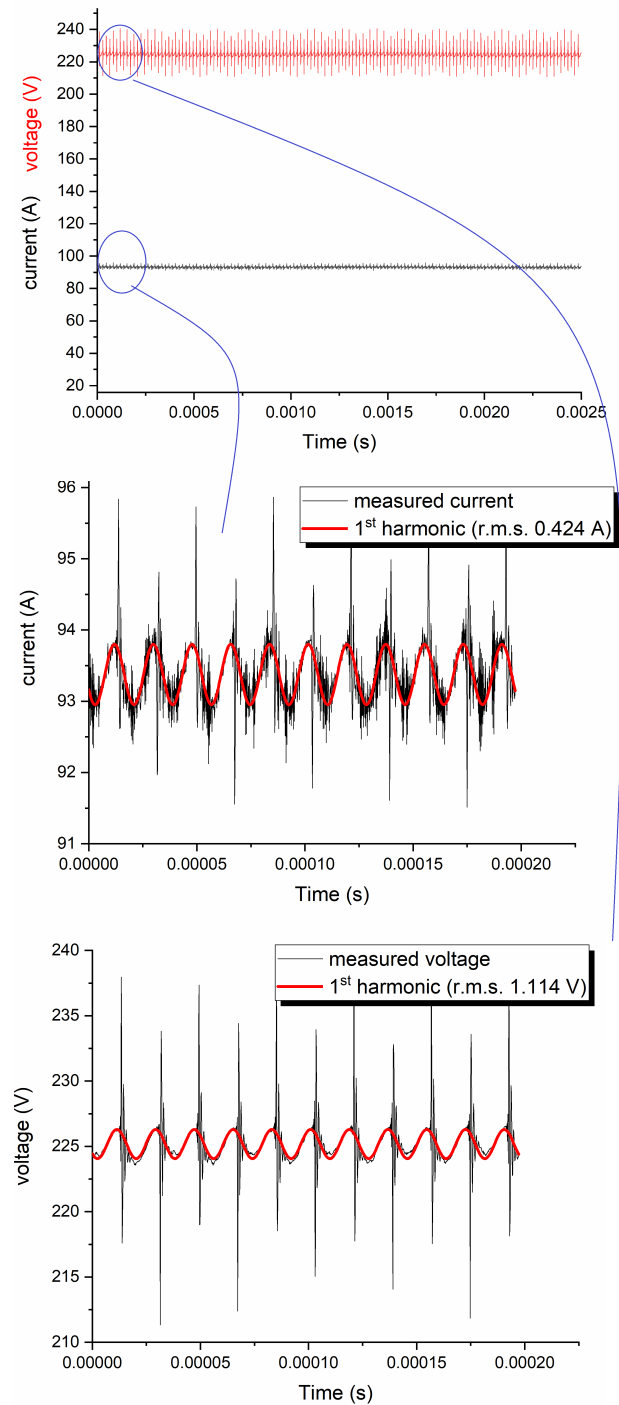| Location at Point E	LVCS	HVCS
Power at the load	3 kW	21 kW
DC currents at the load r.m.s.	30 A	93.8 A
DC voltages at load r.m.s.	100 V	225 V

Figure 5. Voltage and current ripple recorded at HVCS. The frequency is is double with respect to the resonantfrequency of the coils.

3.2. Parameters of Uncertainty

The on-board measurement system includes a Zimmer LG-670 power analyzer, which uses direct voltage input, and current sensor input. The latter makes use of a Guildline 7340 Series, AC-DC Current Calibration Standards coaxial shunts, with a resistance equal to 4 mΩ. As it was highlighted in [20], not all broadband sensors with the same accuracy are suitable for the purpose. The power analyzer and the current transducer considered here provide levels of uncertainty among the best on the market, in the frequency range of interest. Specifications for Zimmer power analyzer are valid in the 20–26 °C range of temperature. Therefore, the basic uncertainty analysis is performed in this range and then extended. The uncertainty components of the electrical power measurement, obtained by means of a sampling system, can be assessed by considerations related to the determination of voltage and current samples and on the basis of the uncertainty of the phase difference detected by the periodic calibrations of the sampling system. A possible solution to assess the uncertainty is to carry out the determination, by means of a Fourier transform (FFT), of the frequency components of the voltages and currents in order to obtain the values. The overall power on-board will be:

$$P_{board}(U_0, I_0, U_1, I_1, U_2, I_2, \phi_2, \ldots) = \sum_{k=0}^{NA} U_k \cdot I_k \cdot \cos \phi_k \tag{2}$$

where U_0 and I_0 are the DC voltage and current respectively, U_i, I_i and ϕ_i are the AC voltage, current and phase angle of the ith harmonic respectively, and NA is the considered number of harmonics of the AC ripple. For the uncertainty calculation, we refer to (2) limiting the analysis to the DC component and the first harmonic of the AC component (ripple). As it will be clearly seen in the following, this is not a significant limitation. In case of uncorrelated components, the related uncertainty on power results as:

$$u_P^2 = \left(u_{\Delta U_0}^2 \cdot I_0^2 + u_{\Delta I_0}^2 \cdot U_0^2 \right) + \left(u_{\Delta U_1}^2 \cdot I_1^2 + u_{\Delta I_1}^2 \cdot U_1^2 \right) \cdot \cos \phi_1{}^2 + u_{\Delta \phi_1}^2 \cdot U_1^2 I_1^2 \sin \phi_1{}^2 \tag{3}$$

being u_P the uncertainty on the measured power, $u_{\Delta U_0}$ and $u_{\Delta I_0}$ the measurement uncertainties on the DC voltage and DC current respectively, and $u_{\Delta U_i}$, $u_{\Delta I_i}$ and $u_{\Delta \phi_0}$ the measurement uncertainties on the AC voltage, current and phase angle of the ith harmonic, respectively. The relative uncertainty on the measured power is consequently:

$$u_{rP} = \frac{u_P}{P_{board}} \tag{4}$$

According to the Zimmer LG670 specifications the channel that measures the shunt voltage (sensor input) is equivalent to the voltage channels. Since the current signal is acquired as a voltage from the sensor input, reference is made to the voltage channel calibration. Calibration results are reported in Table 3, and the referred quantities have the following meaning:

$u_{r\Delta UI_0}$ is the relative uncertainty on the DC voltage;

$u_{r\Delta U}|_{fx\_kHz}$ is the relative uncertainty on the measured voltage in AC at the frequency f_x expressed in kHz;

u_{rU_T} is the relative uncertainty on the measured voltage due to temperature coefficient.

With regard to the sensor input, the quantities considered are similar to those shown in Table 3 and have the same values. These quantities are reported as follows:

$u_{r\Delta UI_0}$ is the relative uncertainty on the voltage measured at the current sensor input in DC;

$u_{r\Delta UI_1}|_{fx\_kHz}$ is the relative uncertainty on the voltage measured at the current sensor input in AC at the frequency f_x expressed in kHz;

u_{rUI_T} is the relative uncertainty on the voltage measured at the current sensor input due to temperature coefficient.

The correlation effect, which is reasonably predominant, is that between the measurement of the DC current and that of the DC voltage. Given that a voltage measurement with an internal reference in the wattmeter was always used, we can assume a full correlation between the two quantities. In AC it can be assumed that the quantities are uncorrelated. Since we pass to the algebraic sum and, given the low impact of the AC component, the estimated uncertainty becomes: $u_{r\Delta UI_0} = u_{r\Delta U_0} = 100$ ppm.

Table 3. Results from power analyzer calibration. Voltage and current sensor input.

Source	Voltage Input Uncertainty Value	Probability Distribution	Coverage Factor	Voltage Input Standard Uncertainty	Voltage Input Standard Uncertainty Value
Uncertainty DC/ppm	100	Normal	2	$u_{r\Delta U_0}$	50
Uncertainty AC 40 kHz/ppm	200	Normal	2	$u_{r\Delta U_1}|_{40\ kHz}$	100
Uncertainty AC 85 kHz/ppm	370	Normal	2	$u_{r\Delta U_1}|_{85\ kHz}$	185
Uncertainty AC 150 kHz/ppm	450	Normal	2	$u_{r\Delta U_1}|_{150\ kHz}$	225
Temperature coefficient/ppm/°C	100	Normal	2	u_{rU_T}	50

Table 4 summarizes the uncertainty parameters and related values concerning the coaxial shunt. The first column summarizes the sources of uncertainty, which are the DC calibration uncertainties and those of AC at different frequencies, the temperature coefficient, the long-term stability for DC measurements and those of AC at different frequencies and, finally, the phase shift at different frequencies. The second column, for each parameter, shows the expanded uncertainty, while the third column shows the probability distribution. Finally, while the fourth column highlights the variable symbol, the last column shows the standard uncertainty value. A detailed definition of several parameters follows:

$u_{r_{\Delta R\_dc}}$　　　　is the DC relative standard uncertainty of the coaxial shunt;

$u_{r_{\Delta R\_dc\_stab}}$　　　is the standard uncertainty related to the DC stability of the shunt;

$u_{r_{\Delta R\_ac\_stab|fxkHz}}$　is the standard uncertainty related to the ac stability of the shunt at the fx frequency in kHz;

$u_{r_{\Delta R\_pow\_coeff}} \times RI^2$　is the standard uncertainty related to the power coefficient R being the shunt resistance.

To build the uncertainty budget according to (3) and (4), the measurement uncertainty related to DC and AC (first harmonic) current components are computed according to (5) and (6):

$$u_{\Delta I_0} = I_0 \sqrt{u_{r\Delta UI_0}^2 + u_{r\Delta R}^2} \tag{5}$$

$$u_{\Delta I_1} = I_1 \sqrt{u_{r\Delta UI_1}^2 + u_{r\Delta R_1}^2} \tag{6}$$

where

$$u_{r\Delta R} = \sqrt{u_{r_{\Delta R\_dc}}^2 + u_{r_{\Delta R\_dc\_stab}}^2 + \left(u_{r_{\Delta R\_pow\_coeff}} \cdot RI_0^2\right)^2} \tag{7}$$

$$u_{r\Delta R_1} = \sqrt{u_{r_{\Delta R_{fx}}}^2 + u_{r_{\Delta R\_ac\_stab|fx}}^2 + \left(u_{r_{\Delta R\_pow\_coeff}} \cdot RI_1^2\right)^2} \tag{8}$$

fx being the frequency of the first harmonic. Using the measured voltage and the results of Table 3, the measured currents and the results of Table 4, together with formulas from (5) to (8), it is possible to compute the uncertainty parameters to be implemented in (3) to obtain the uncertainty on the power measurement in the case of the LVCS, load condition #1. The process of the uncertainty computation is summarized in Figure 6.

Table 4. Coaxial shunt uncertainty parameters.

Uncertainty Source	Shunt Expanded Uncertainty	Probability Distribution	Standard Uncertainty Parameter	Standard Uncertainty Value
DC/ppm	17	Normal	$u_{r_{\Delta R\_dc}}$	8.5
AC 40 kHz/ppm	47	Normal	$u_{r_{\Delta R\_ac}\|40\text{ kHz}}$	23.5
AC 85 kHz/ppm	80	Normal	$u_{r_{\Delta R\_ac}\|85\text{ kHz}}$	40
AC 150 kHz/ppm	130	Normal	$u_{r_{\Delta R\_ac}\|150\text{ kHz}}$	65
Temp. coeff./ppm/C	4.5	Normal	$u_{r_{Rs}}$	2.25
Power coeff./ppm/W	6	Normal	$u_{r_{\Delta R\_pow\_coeff}}$	3
Long term stability @DC/ppm	16 [**]	Normal	$u_{r_{\Delta R\_dc\_stab}}$	8
Long term stability @40 kHz/ppm	140 [**]	Normal	$u_{r_{\Delta R\_ac\_stab}\|40\text{ kHz}}$	70
Long term stability @85 kHz/ppm	280 [**]	Normal	$u_{r_{\Delta R\_ac\_stab}\|85\text{ kHz}}$	140
Long term stability @150 kHz/ppm	370 [**]	Normal	$u_{r_{\Delta R\_ac\_stab}\|150\text{ kHz}}$	185
Phase shift (rad) @40 kHz	1.2×10^{-3} [**]	Rectangular	$u_{\Delta\phi\|40\text{ kHz}}$	0.70×10^{-3}
Phase shift (rad) @85 kHz	2.3×10^{-3} [**]	Rectangular	$u_{\Delta\phi\|85\text{ kHz}}$	1.31×10^{-3}
Phase shift (rad) @150 kHz	3.8×10^{-3} [**]	Rectangular	$u_{\Delta\phi\|150\text{ kHz}}$	2.22×10^{-3}

[**] Derived from extrapolation from datasheet.

The results of the computation are reported in Table 5 in which the last line shows the relative uncertainty, referred to as the measured power. Notably, in Table 5 the AC component (first harmonic) produces negligible contributions (this happens for both stations in both charging conditions), which justifies the simplification made in Formula (2), for which the other harmonic components are neglected. A detailed table is not reported for the other station and load conditions, but the results in terms of expanded relative uncertainty on the measured power are illustrated in Table 6. It can be seen that although the charging stations are very different, the expanded measurement uncertainty is identical and equal to 300 ppm for both EVSEs in the first load condition, and slightly higher (by 20 ppm) for the HVCS in the second load condition.

Table 5. Uncertainty budget. LVCS, #1. The parameter distributions are normal.

Parameter	Value	Sensitivity Coefficient	Sensitivity Coefficient Value	Contribution (W)
$u_{\Delta U_0}$	0.01126 V	I_0	27.4 A	0.26723
$u_{\Delta I_0}$	0.00319 A	U_0	97.5 V	0.27012
$u_{\Delta U_1}$	9.353×10^{-5} V	$I_1 \times \cos\phi_1$	1.2786 A	1.0357×10^{-4}
$u_{\Delta I_1}$	2.379×10^{-4} A	$U_1 \times \cos\phi_1$	0.80911 V	1.8293×10^{-4}
$u_{\Delta\phi_1}$	1.60×10^{-3}	$U_1 \times I_1 \times \sin\phi_1$	0.04862	7.780×10^{-5}

Total standard uncertainty 0.3800 W. Total power 2627.5 W. Standard relative uncertainty 144.6 ppm approx. @150 ppm.

Table 6. Computed expanded uncertainties, measurements on-board.

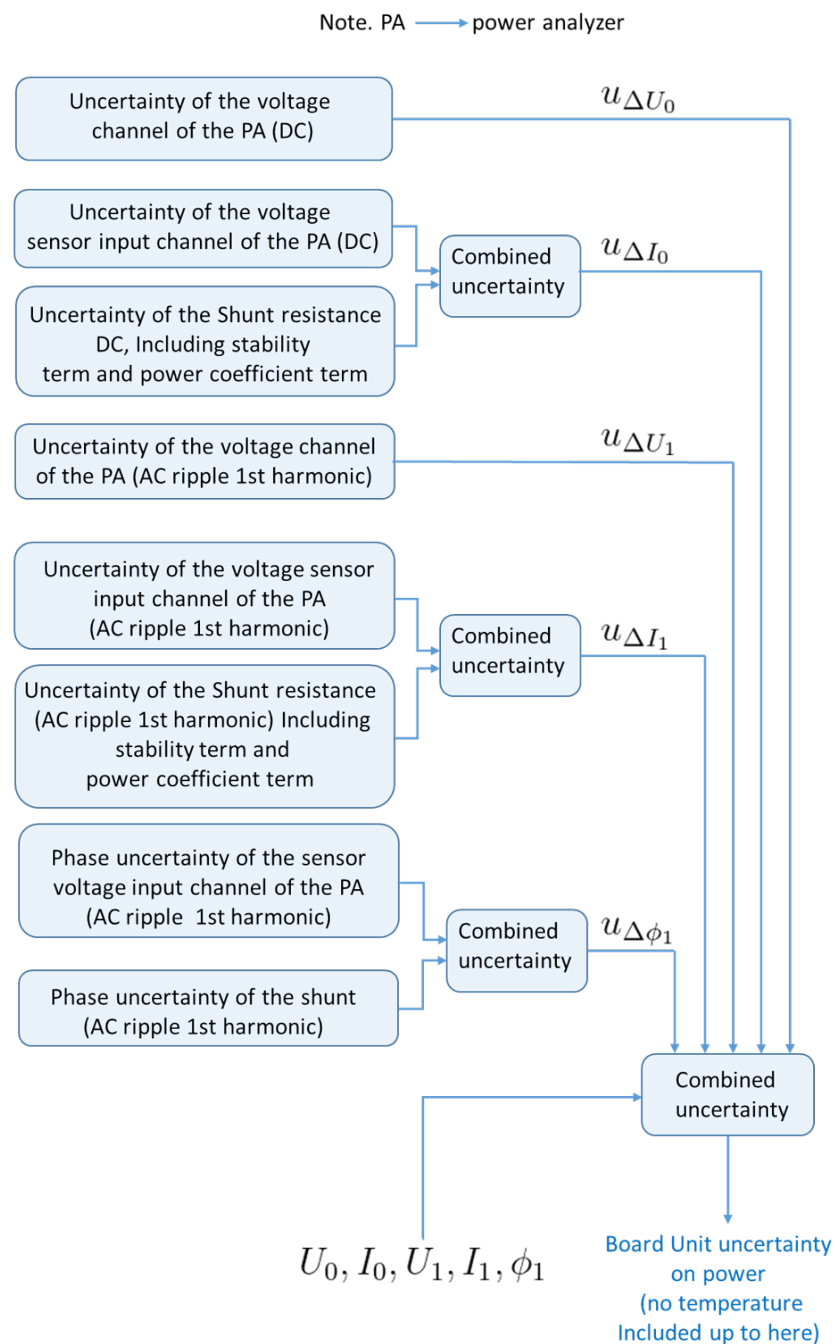| Station	Load Condition	Expanded Uncertainty/ppm
LVCS	#1	300
LVCS	#2	300
HVCS	#1	300
HVCS	#2	320

Figure 6. Uncertainty computation process for the BU.

4. Grid Side Measurements and Parameters of Uncertainty

The maximum values of voltage, current, and adsorbed power recorded during the measurements at the grid (point A, Figure 4), are shown in Table 7. The recorded values show a sinusoidal voltage with minimal local distortions, while the current waveforms suffer from a significant distortion due to disturbances from the power converters. Figure 7 shows the waveforms recorded at HVCS; analogous waveforms were recorded at LVCS. The grid side measurement uncertainty is based on the laboratory performed calibration of the Yokogawa WT-3000 power analyzer together with the Yokogawa LEM 65-S and 205-s Ultrastab current transducers.

Table 7. Maximum measured quantities at the grid connection point.

Location at Point A	LVCS	HVCS
Power absorbed from the grid	3.0 kW	27.4 kW
Phase currents r.m.s.	5.2 A	38.5 A
Phase voltages r.m.s.	222.0 V	238.6 V
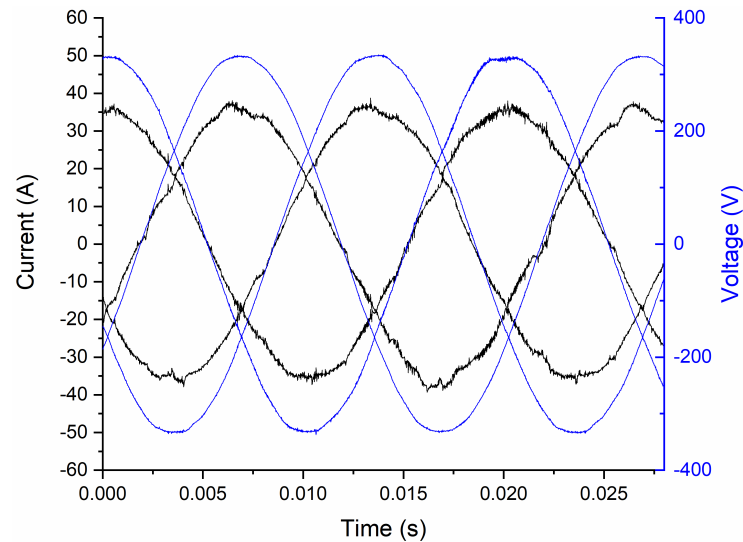
Figure 7. Three phase grid voltages and currents recorded at HVCS. Load condition #2, Table 1.

The calculation of the uncertainty is performed for all the phases. We name the three phases ρ, σ, and τ. In the following, for simplicity, the first phase (ρ) is considered to be extending the result to the other phases.

$$U_{\rho grid}\left(U_{\rho1}, \phi_{u\rho1}, U_{\rho2}, \phi_{u\rho2}, \ldots\right) = U_{\rho0} + \sum_{k=1}^{n} U_{\rho k} \cdot \left(\cos k\omega t + \phi_{u\rho k}\right) \tag{9}$$

$$I_{\rho grid}\left(I_{\rho1}, \phi_{i\rho1}, I_{\rho2}, \phi_{i\rho2}, \ldots\right) = I_{\rho0} + \sum_{k=1}^{n} I_{\rho k} \cdot \left(\cos k\omega t + \phi_{i\rho k}\right) \tag{10}$$

$$P_{\rho1} = P_{\rho\_fund} = U_{\rho1} \cdot I_{\rho1} \cdot \cos \Delta\phi_{\rho1} \tag{11}$$

The distortion power, for each phase, can be computed as the difference between the measured power and the first harmonic (or fundamental) power:

$$P_{\rho\_distortion} = P_{\rho\_meas} - P_{\rho\_fund} \tag{12}$$

$$\Delta P_{distortion} = P_{\rho\_distortion} + P_{\sigma\_distortion} + P_{\tau\_distortion} \tag{13}$$

$$P_{fund} = P_{\rho\_fund} + P_{\sigma\_fund} + P_{\tau\_fund} \tag{14}$$

The uncertainty due to the harmonic distortion can be expressed as:

$$u_{rP\_distortion} = \frac{|\Delta P_{distortion}|}{\sqrt{3} \cdot P_{fund}} \tag{15}$$

Taking all distorted power as uncertainty is to follow a conservative approach. In the author's opinion, such an approach is a good practice when, as in the analyzed cases, data on calibration beyond the power frequency are not available, which commonly happens in current calibrations at power frequency. According to formula (15) the computed values in ppm are reported in the following:

LVCS: #1 → 123 ppm, #2 → 224 ppm.
HVCS: #1 → 108 ppm, #2 → 83 ppm.

The uncertainty parameters for grid measurements are shown in Table 8. They are: (i) the uncertainty of the power analyzer, (ii) the uncertainty due to the harmonic distortion which has just been discussed and (iii) the uncertainty due to the temperature. Neglecting this last parameter, which will be discussed in the next section, since the standard uncertainty of the power analyzer is only 25 ppm, making reference to the worst case, at room temperature, the composed standard measurement uncertainty at the grid side is $u_{r_{Pgrid}} = 225$ ppm for LVCS and $u_{r_{Pgrid}} = 110$ ppm for HVCS.

Table 8. Uncertainty components related to power grid measurement.

Uncertainty Factor	Uncertainty Source	Expanded Uncertainty /ppm	Coverage Factor	Current Input Standard Uncertainty	Standard Uncertainty /ppm
Power analyzer accuracy	Calibration certificate	50	2	$u_{r_{Pgrid\_cal}}$	25
Uncertainty variation vs temperature	WT3000 and LEM specifications	202/C	$\sqrt{3}$	$u_{r_{Pgrid\_temp}}$	116.6/C
Uncertainty due to harmonic content	Computed $\frac{\Delta P_{distortion}}{P_{fund}}$	(*)	$\sqrt{3}$	$u_{r_{Pgrid\_distortion}}$	(**)

(*) Specific computations in this section. (**) 224 ppm for LVCS and 108 ppm for HVCS.

5. Overall Efficiency Measurement Uncertainty and Temperature Effect

5.1. The Grid Side Temperature Effect

Concerning the grid measurements, the calibration uncertainty is considered valid in the temperature range 22 °C $\leq T \leq$ 24 °C. Therefore the grid side temperature variation $\Delta\theta$ is defined as follows:

$$\forall \theta^* < 22\,°C \qquad \Delta\theta = 22\,°C - \theta^* \tag{16}$$

$$\forall \theta^* > 24\,°C \qquad \Delta\theta = \theta^* - 24\,°C \tag{17}$$

The final standard relative uncertainty is then computed as:

$$u_{r_{Pgrid}} = \sqrt{(u_{r_{Pgrid}})^2_{cal} + (u_{P_{grid\_Temp}} \times \Delta\theta)^2 + (u_{r_{Pgrid\_distortion}})^2} \tag{18}$$

and the values at room temperature are reported in the previous section.

5.2. The On-Board Side Temperature Effect

Concerning on-board measurements, according to LMG670 specification outside the temperature range 20 °C $\leq T \leq$ 26 °C, the voltage and current temperature coefficients are not negligible and must be considered.

$$\forall T^* < 20\,°C \qquad \Delta T = 20\,°C - T^* \tag{19}$$

$$\forall T^* > 26\,°C \qquad \Delta T = T^* - 24\,°C \tag{20}$$

$$P_{board} = P_{board}(U_0, I_0, T, R_s) = U_0(T) \times \frac{U_s(T)}{R_s(T)} + \ldots \tag{21}$$

$$\frac{\partial P_{board}}{\partial T} = \frac{U_0(T)}{R_s(T)} \times \frac{\partial U_s(T)}{\partial T} + \frac{U_s(T)}{R_s(T)} \times \frac{\partial U_0(T)}{\partial T} + $$
$$- U_0(T) \times U_s(T) \times \frac{1}{R_s^2(T)} \times \frac{\partial R_s(T)}{\partial T} + \ldots \tag{22}$$

$$\frac{1}{P_{board}} \times \frac{\partial P_{board}}{\partial T} = \frac{1}{U_s(T)} \times \frac{\partial U_s(T)}{\partial T} + \frac{1}{U_0(T)} \times \frac{\partial U_0(T)}{\partial T} - \frac{1}{R_s} \times \frac{\partial R_s(T)}{\partial T} \tag{23}$$

As discussed in Section 4, the contribution of the AC components to the uncertainty of the measurement at the batteries on-board is negligible despite the ripple. Therefore, the variation of the additional relative uncertainty with temperature from (23) is made explicit in Formula (24). This is part of the uncertainty evaluation and is zero when ΔT is equal to zero.

$$\frac{\Delta u_{rP_{board}}(T)}{\Delta T} = \frac{1}{\Delta T} \times \sqrt{u_{rU_s}^2(T) + u_{rU_0}^2(T) + 2ru_{rU_s}(T) \times u_{rU_0}(T) + u_{rR_s}^2(T)} \tag{24}$$

The complete expression of the uncertainty related to the measurements on-board is then:

$$u_{rP_{board}}(T) = \sqrt{u_{rP_{board}}^2 + \left(\frac{\Delta u_{rP_{board}}(T)}{\Delta T} \times \Delta T\right)^2} \tag{25}$$

where $u_{rP_{board}}$ is computed in Section 4, and the related expanded uncertainties are reported in Table 6.

5.3. The Overall Efficiency Uncertainty

The uncertainty of the overall efficiency was computed versus temperature and the results are reported in Table 9, with reference to the worst case of the LVCS station. The table shows in the first and second columns the measurement temperatures equidistant from the room temperature range. The third column illustrates the uncertainty calculated in the measurement on-board, starting from the uncertainty calculated at room temperature (see Section 5.2). The fourth column reports the uncertainty of the measurement of the grid power. The fifth column shows the uncertainty related to the overall efficiency measurement, computed with formula (1). Finally, the last column reports the expanded uncertainty, with coverage factor $k = 2$. The analysis of the expanded measurement uncertainty shows that the target 10^{-3} can be achieved in the temperature range 18 °C $\leq T \leq$ 28 °C for LVCS. The analysis on the HVCS, not reported here for brevity, shows that the target is reached in the range 17 °C $\leq$ T $\leq$ 29 °C . For the measurement of the power the target is reached in the range 14 °C $\leq T \leq$ 32 °C for both stations. We can therefore conclude that the values reported in Table 9 are conservative; furthermore, although the two charging stations have very different power levels, the results regarding the uncertainty evaluation are absolutely similar. Finally, it is worth noting that the reference measurement system can perform measurements in a wide range of temperatures, i.e., between 5 °C and 40 °C with an expanded uncertainty within 0.5%.

Table 9. Overall efficiency uncertainty vs temperature LVCS worst case.

T /°C	T /°C	On-Board SU $u_{rP_{board}}(T)$/ppm	Grid SU $u_{rP_{grid}}(T)$/ppm	Efficiency SU $u_\mu(T)$/ppm	Expanded Uncertainty $U_\mu(T)$/‰
5	41	1235	1994	2087	4.17
6	40	1154	1879	1963	3.93
10	36	831	1417	1462	2.92
11	35	750	1302	1337	2.67
14	32	513	959	968	1.94
15	31	435	846	847	1.69
16	30	360	735	728	1.46
17	29	287	625	612	1.22
18	28	222	518	502	1.00
20	26	150	324	318	0.64
21	25	150	253	262	0.52
23	24	150	225	241	0.48

SU means Standard Uncertainty. Efficiency $\mu = 0.89$.

6. Charging Stations Bench-Marking

To the authors' knowledge, there are no specific regulations for inductive charging stations that specify the accuracy of the power measurement for the installed instrumentation. For this reason, the investigation on the accuracy of the installed measurement systems at the station is a necessary step. The measurement systems implemented in the two considered EVSEs were evaluated by comparison with the standard measurement system described in this paper. Measurements at LVCS were performed in a laboratory environment (temperature is not an issue) while measurements at HVCS were performed at the beginning of October with daily temperatures in the range of $18\,°C \le T \le 25\,°C$, respecting the limits discussed in Section 5.

Benchmarking measurements were performed at two different power levels for each station, repeating measurements three times for each working condition. The repetition was done restarting the stations power supply each time; therefore, the three results do not show the repeatability of the measurements, but rather the ability of the station power supply system and control in repeating the same power supply conditions.

The expected result of the comparison, in accordance with the few regulations in force (such as e.g., ANSI C12.20, or EN 50463-2 for railway transport) should show relative discrepancies not exceeding 0.5%.

The comparison at LVCS is presented in Table 10 with aligned coils and in Table 11 with misaligned coils. The two tables are organized as follows: the second column provides the overall efficiency measured with the EVSE measurement system, while the third column provides the measurement obtained with the standard measurement system analyzed in this paper. The fourth and fifth columns provide the relative percentage difference between the results provided by the two measurement systems regarding the power measured on board and the power measured at the grid connection, respectively. Finally, the last column provides the relative percentage difference on the overall efficiency.

The comparisons provide results with discrepancies always lower than 0.5%. The charging station, as expected, shows a better performance when the load condition is close to the nominal one, and the performance worsens, as expected, in the case of misaligned coils. Also, the measurement results are in better agreement in case of higher load conditions and this is due to the range of the current transducers installed at the charging station that in lower load conditions, are at the limit of the minimum range.

Table 10. Measurement Comparison at LVCS. Aligned Coils.

n	LVCS $\mu_{tot} = \dfrac{P_L}{P_g}$	Standard $\mu_{tot} = \dfrac{P_L}{P_g}$	Relative Difference %P_L	Relative Difference %P_{grid}	Relative Difference %$\lvert \mu_{tot} \rvert$
1	73.736	73.506	0.43	0.15	0.31
2	73.817	73.531	0.34	0.04	0.39
3	73.587	73.413	0.29	0.06	0.24
4	89.232	88.978	0.01	0.27	0.29
5	89.378	89.117	0.19	0.46	0.29
6	89.414	89.131	0.12	0.42	0.32

Table 11. Measurement Comparison at LVCS. Misaligned Coils.

n	LVCS $\mu_{tot} = \dfrac{P_L}{P_g}$	Standard $\mu_{tot} = \dfrac{P_L}{P_g}$	Relative Difference %P_L	Relative Difference %P_{grid}	Relative Difference %$\lvert \mu_{tot} \rvert$
1	66.098	65.857	−0.39	0.06	0.37
2	66.052	65.788	−0.25	0.12	0.40
3	66.548	66.284	−0.35	0.04	0.40
4	85.825	85.648	−0.01	0.19	0.21
5	85.785	85.572	−0.13	0.11	0.25
6	85.777	85.523	−0.10	0.18	0.30

The comparison at the HVCS is shown in Table 12, which has the same structure as the previous two. The comparison of the measured power at the electrical grid gives good results, which are better when the load approaches the nominal one. The comparison of the measurement on-board, on the other hand, provided unexpected results with increasing discrepancies with the load and in excess up to about 5%. From a subsequent investigation on the installed transducer at the EVSE LVCS, this discrepancy resulted in being due to an unexpected drift of the current transducer on-board. The transducer, which was subsequently replaced, has led to a measurement of the efficiency lower than the real one.

Table 12. Measurement Comparison at HVCS.

n	LVCS $\mu_{tot} = \dfrac{P_L}{P_g}$	Standard $\mu_{tot} = \dfrac{P_L}{P_g}$	Relative Difference %P_L	Relative Difference %P_{grid}	Relative Difference %$\lvert \mu_{tot} \rvert$
1	71.955	73.507	2.51	0.41	2.11
2	71.387	73.137	2.70	0.31	2.39
3	71.585	73.465	2.78	0.19	2.56
4	73.451	77.298	5.15	0.18	4.98
5	73.118	76.898	5.12	0.21	4.92
6	73.030	76.850	5.12	0.16	4.97

In conclusion, the overall result of the survey underlines that class 0.5 can be a reasonable target for measuring systems mounted at WPT EVSEs and that on-site verification of measuring systems is certainly desirable.

7. Measurements at the Resonant Circuit

The measurements at the resonant circuit are interesting with regard to evaluating the actual power transferred to the vehicle, net of losses in the converters. Moreover, the measurements of the coil currents are indirectly useful for the dosimetric evaluation of human exposure to the magnetic fields produced by resonant coils [27]. In this section we discuss a reasonable uncertainty target for these measurements, which arises from the analysis of the waveforms measured on-site. The target is different from that for measuring overall efficiency, as voltage and current have a more important harmonic distortion in this part of the EVSE WPT system.

Though the type of resonant circuits may be different in both the stations analyzed, the voltage shows a rectangular waveform and the current is sinusoidal with a content mainly including a third and fifth harmonic, plus some high frequency noise, as shown in Figure 8. The rectangular waveform of the voltage is obtained close to the rated load, while as the load is reduced the voltage becomes an eight-step voltage which shrinks by reducing the transmitted/received power. Two waveforms and the typical spectrum are shown in Figure 9. In the LVCS, the third (0.81% of the 1st harmonic) and fifth (0.10% of the 1st harmonic) harmonics make the current signal more pointed (it tends to resemble a triangular waveform) as the load approaches the rated power. In the HVCS the harmonics in the waveform of the current (third 1.8% and fifth 0.57% of the 1st harmonic) compose showing a slight concavity on the rising edge and a slight convexity on the falling edge. The harmonic contributions, especially the third and fifth harmonics, weigh significantly in the power measurement. Furthermore, in the case of LVCS, these harmonics occurs at around 170 kHz for the third and 255 kHz for the fifth harmonic, i.e., in a frequency range where traceability of the power is an issue. Following the conservative approach proposed in Formula (15), the distortion power can be considered an uncertainty term. In the case of LVCS the power related to harmonics represents a non-negligible uncertainty contribution. We can compute the related relative uncertainty as:

$$u_{rP_{distortion}} = \frac{\lvert \Delta P_{distortion} \rvert}{\sqrt{3} \times P_{fund}} = \frac{3.205}{\sqrt{3} \times 2980.45} = 621 \text{ ppm} \tag{26}$$

and then

$$u_{rResonant} = \sqrt{u_{rP_{fund}}{}^2 + u_{rP_{distortion}}{}^2} = \sqrt{570^2 + 621^2} = 842.9 \text{ ppm} \qquad (27)$$

approximated to 850 ppm. The relative expanded uncertainty, assuming a coverage factor equal to $k = 2$, is 0.17% at room temperature. Similar figures have been found at both stations. It can therefore be concluded that the measurement of the power transmitted or received on-board in the resonant circuits may be subjected to a measurement uncertainty equal to or greater than 0.2%, which depends on the type and architecture of the resonant circuit, working frequency and the relative harmonic distortion.
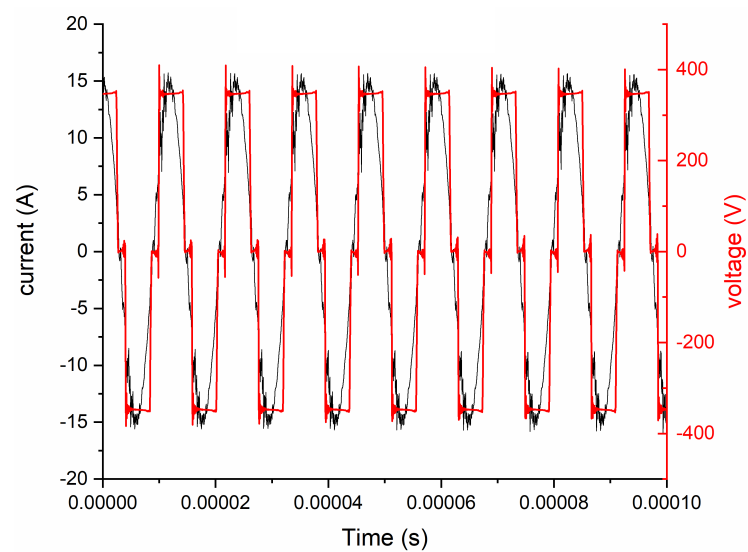
Figure 8. Current and voltage at the LVCS transmitter coil.

(**a**)

Figure 9. *Cont.*

(**b**)
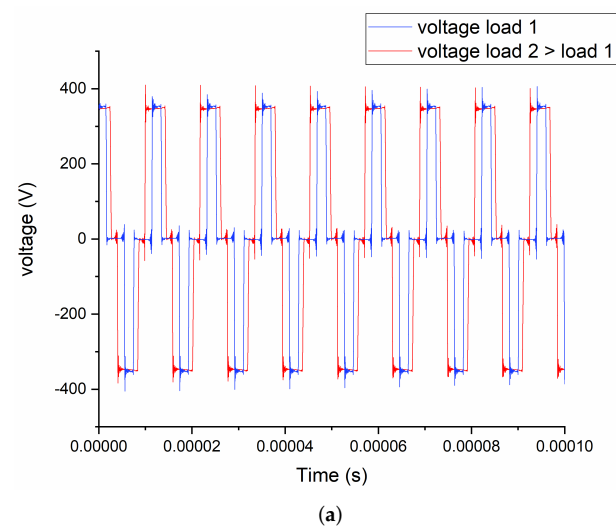
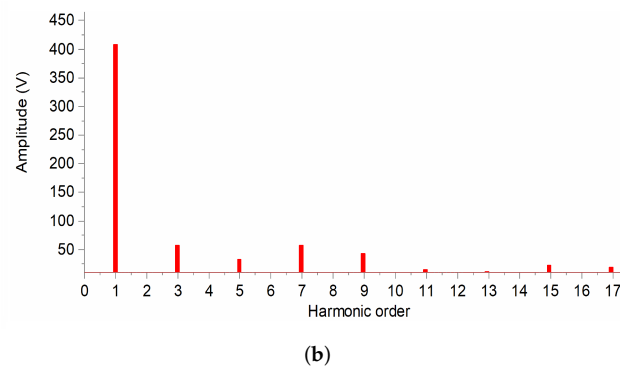**Figure 9.** (**a**) Voltage at LVCS transmitter coil (two load conditions). (**b**) FFT spectrum of the voltage in the resonant circuit (load 2 in Figure 8a).

8. Conclusions

This study analyzed the measurement of electrical power and overall efficiency performed on-site at a WPT EVSE. A reference measurement system composed of two subsystems was used: one for on-board measurements and one for measurements at the grid connection point. Both subsystems had been previously calibrated; the one for on-site measurements with DC + AC (ripple) waveforms up to 150 kHz, the second was calibrated at the grid frequency and both provided an expanded measurement uncertainty better than 0.1%. Although the architecture of the power converters may be different in specific cases, the analysis of the on-site waveforms showed that the voltage and current ripple can have a frequency that is double of the transmission frequency of the EVSE, and this has to be kept in mind in the calibration. This paper discussed how the measurement uncertainty of the standard measurement system may or may not be maintained in on-site measurements. To do this, a method was proposed by this paper that takes advantage of the waveforms measured at two WPT EVSEs of very different power, and introduced the uncertainty terms deriving from the harmonic distortion of the waveforms and the temperature variation. The obtained result underlined that the extended measurement uncertainty of 0.1% is maintained for the grid power measurement, for on-board power measurement and for the assessment of the overall efficiency, in a temperature range of between 18 °C and 28 °C, which is even greater for one of the two EVSE's.The same measurement system provide a measurement uncertainty below 0.5% between 5 °C and 17 °C and between 29 °C and 40 °C. A second step of the study was the assessment of the measurement uncertainty of the instrumentation mounted at the EVSE. Operating in the temperature span providing the better measurement accuracy, the existing measurement system at the EVSEs were analyzed: LVCS provided discrepancies on power measured on-board and on the power measured at the grid connection point, as well as the measured overall efficiency, lower than 0.5%. Measurements at HVCS showed the same results at the grid side but shown an anomalous drift on a current transducer installed at the station. The observed results underline that the class 0.5 for the instrumentation at the WPT EVSE can be suitable, as already envisaged by the standards for similar applications such as railways. Another result obtained from the study was the quantification of the power associated with the voltage and current ripple at the batteries, which although it appears visually significant at the sight of the waveforms, counts for less than 0.1% of the power transferred to the load. Finally, the study highlighted that given the frequencies involved and the high harmonic distortion, the on-site measurements at the resonant circuit require further investigation and that considering the high level of the distorted waveforms and their influence on the uncertainty, the measurement uncertainty of 0.1% at laboratory temperature cannot be reached on-site, but it is conservative to consider an extended uncertainty of at least double.

Author Contributions: Conceptualization, M.Z., U.P. and V.C.; methodology, M.Z. and U.P.; formal analysis, M.Z. and U.P.; investigation, M.Z., V.C., J.B., D.S., E.L., M.A.A.T. and F.F.; resources, V.C., J.B., E.L., J.C., D.S. and M.A.A.T.; data curation, M.Z., U.P., J.B. and V.C.; writing—original draft

References

1. Ding, X.; Wang, Z.; Zhang, L. Hybrid Control-Based Acceleration Slip Regulation for Four-Wheel-Independently-Actuated Electric Vehicles. *IEEE Trans. Transp. Electrif.* **2020**. [CrossRef]
2. Wang, C.; Wang, Z.; Zhang, L.; Cao, D.; Dorrell, D.G. A Vehicle Rollover Evaluation System Based on Enabling State and Parameter Estimation. *IEEE Trans. Ind. Inform.* **2020**. [CrossRef]
3. Ding, X.; Wang, Z.; Zhang, L.; Wang, C. Longitudinal Vehicle Speed Estimation for Four-Wheel-Independently-Actuated Electric Vehicles Based on Multi-Sensor Fusion. *IEEE Trans. Veh. Technol.* **2020**, *69*, 12797–12806. [CrossRef]
4. Ghosh, A. Possibilities and Challenges for the Inclusion of the Electric Vehicle (EV) to Reduce the Carbon Footprint in the Transport Sector: A Review. *Energies* **2020**, *13*, 602. [CrossRef]
5. Sayed, K.; Kassem, A.; Saleeb, H.; Alghamdi, A.S.; Abo-Khalil, A.G. Energy-Saving of Battery Electric Vehicle Powertrain and Efficiency Improvement during Different Standard Driving Cycles. *Sustainability* **2020**, *12*, 10466. [CrossRef]
6. Kishan, D.; Nayak, P.S.R. Wireless power transfer technologies for electric vehicle battery charging—A state of the art. In Proceedings of the 2016 International Conference on Signal Processing, Communication, Power and Embedded System (SCOPES), Odisha, India, 3–4 October 2016; pp. 2069–2073. [CrossRef]
7. Cirimele, V.; Diana, M.; Freschi, F.; Mitolo, M. Inductive Power Transfer for Automotive Applications: State-of-the-Art and Future Trends. *IEEE Trans. Ind. Appl.* **2018**, *54*, 4069–4079.
8. Amin, A.; Tareen, W.U.K.; Usman, M.; Memon, K.A.; Horan, B.; Mahmood, A.; Mekhilef, S. An Integrated Approach to Optimal Charging Scheduling of Electric Vehicles Integrated with Improved Medium-Voltage Network Reconfiguration for Power Loss Minimization. *Sustainability* **2020**, *12*, 9211. [CrossRef]
9. Ferwerda, R.; Bayings, M.; van der Kam, M.; Bekkers, R. Advancing E-Roaming in Europe: Towards a Single Language for the European Charging Infrastructure. *World Electr. Veh. J.* **2018**, *9*, 50. [CrossRef]
10. Ma, C.T. System planning of grid-connected electric vehicle charging stations and key technologies: A review. *Energies* **2019**, *12*, 4201. [CrossRef]
11. Knez, M.; Zevnik, G.K.; Obrecht, M. A review of available chargers for electric vehicles: United States of America, European Union, and Asia. *Renew. Sustain. Energy Rev.* **2019**, *109*, 284–293. [CrossRef]
12. Kim, J.D. Insights into residential EV charging behavior using energy meter data. *Energy Policy* **2019**, *129*, 610–618. [CrossRef]
13. Stoychev, I.; Tebbe, J.; Oehm, J. A measurement system for electric car charging stations utilising a FPGA board for flexibility in configuration. In Proceedings of the IEEE International Symposium on Circuits and Systems (ISCAS), Montréal, QC, Canada, 22–25 May 2016; pp. 630–633. [CrossRef]
14. Rajendran, G.; Vaithilingam, C.A.; Naidu, K. Energy-efficient converters for electric vehicle charging stations. *SN Appl. Sci.* **2020**, *2*, 1–15. [CrossRef]
15. Lodetti, S.; Bruna, J.; Sanz, J.F.; Melero, J.J. Characterization of the Emission of an Electric Bus Inductive Charging in the 2 kHz to 150 kHz Range. In Proceedings of the AEIT International Conference of Electrical and Electronic Technologies for Automotive (AEIT AUTOMOTIVE), Turin, Italy, 2–4 July 2019; pp. 1–6.
16. Chu, S.Y.; Avestruz, A.-T. Transfer-power measurement: A non-contact method for fair and accurate metering of wireless power transfer in electric vehicles. In Proceedings of the IEEE 18th Workshop on Control and Modeling for Power Electronics, Stanford, CA, USA, 9–12 July 2017; pp. 1–8. [CrossRef]
17. Zucca, M.; Squillari, P.; Pogliano, U. A measurement system for the characterization of wireless charging stations for electric vehicles. In Proceedings of the 2020 Conference on Precision Electromagnetic Measurements (CPEM), Denver, CO, USA, 24–28 August 2020; pp. 1–2. [CrossRef]
18. Zucca, M.; Squillari, P.; Pogliano, U. A measurement system for the characterization of wireless charging stations for electric vehicles. *IEEE Trans. Instrum. Meas.* **2021**, *70*, 1–10.

19. Lucas, A.; Trentadue, G.; Scholz, H.; Otura, M. Power quality performance of fast-charging under extreme temperature conditions. *Energies* **2018**, *11*, 2635. [CrossRef]

20. Zucca, M. Metrology for Inductive Charging of Electric Vehicles (MICEV). In Proceedings of the AEIT International Conference of Electrical and Electronic Technologies for Automotive (AEIT AUTOMOTIVE), Turin, Italy, 2–4 July 2019; pp. 1–4. [CrossRef]

21. Zucca, M. Electrical measurements at inductive charging stations for electric vehicles. An outcome from Micev project. In Proceedings of the Conference on Precision Electromagnetic Measurements (CPEM 2020), Denver, CO, USA, 24–28 August 2020; pp. 1–2. [CrossRef]

22. Ahmad, A.; Alam, M.S.; Chabaan, R. A Comprehensive Review of Wireless Charging Technologies for Electric Vehicles. *IEEE Trans. Transp. Electrif.* **2018**, *4*, 38–63.

23. VICTORIA Project. Available online: https://www.fcirce.es/en/smart-mobility-en-en/victoria-2 (accessed on 23 February 2021).

24. Cirimele, V. The Fabric ICT Platform for Managing Wireless Dynamic Charging Road Lanes. *IEEE Trans. Veh. Technol.* **2020**, *69*, 2501–2512. [CrossRef]

25. Bucci, G.; Ciancetta, F.; Fiorucci, E.; Ometto, A. Uncertainty Issues in Direct and Indirect Efficiency Determination for Three-Phase Induction Motors: Remarks About the IEC 60034-2-1 Standard. *IEEE Trans. Instrum. Meas.* **2016**, *65*, 2701–2716.

26. Möller, F.; Müller, S.; Meyer, J. Impact of Electric Vehicles on Power Quality in Central Charging Infrastructures. In Proceedings of the 1st E-Mobility Power System Integration Symposium, Berlin, Germany, 24–27 October 2017. [CrossRef]

27. Liorni, I. Assessment of Exposure to Electric Vehicle Inductive Power Transfer Systems: Experimental Measurements and Numerical Dosimetry. *Sustainability* **2020**, *12*, 4573. [CrossRef]